Received: 25 November 2022 | Revised: 16 February 2023 | Accepted: 25 February 2023

DOI: 10.1002/inf2.12418

RESEARCH ARTICLE

WILEY

Scalable van der Waals graphene films for electro-optical regulation and thermal camouflage

Ziqi Li[1,2] | **Xujiang Chao**[3] | **Andrew Balilonda**[1] | **Wei Chen**[1,2]

[1]Research Institute for Intelligent Wearable Systems, The Hong Kong Polytechnic University, Hong Kong, the People's Republic of China

[2]The Hong Kong Polytechnic University Shenzhen Research Institute, Shenzhen, the People's Republic of China

[3]School of Mechanical Engineering, Northwestern Polytechnical University, Xian, Shaanxi, the People's Republic of China

Correspondence
Wei Chen, Research Institute for Intelligent Wearable Systems, The Hong Kong Polytechnic University, Hong Kong, 999077, the People's Republic of China.
Email: weii.chen@polyu.edu.hk

Funding information
Shenzhen-Hong Kong-Macao Science and Technology Plan Project, Grant/Award Number: SGDX2020110309520101; Research Grants Council of Hong Kong, Grant/Award Number: 15302121; National Natural Science Foundation of China, Grant/Award Number: 21975214; National Key R&D Program of China, Grant/Award Number: 2018YFC2000900; Seed Fund of Research Institute of Intelligent Wearable Systems (CD45); Start-up Fund of The Hong Kong Polytechnic University (BE1H); Departmental General Research Fund of The Hong Kong Polytechnic University (UAME)

Abstract

Graphene exhibits enormous advantages in mid-infrared (MIR) regulation because of the active control, precise regulation, and large modulation depth. Such graphene films are prepared via chemical vapor deposition (CVD) or reduction, which cannot realize large-scale production and limit the applications. Graphene films with van der Waals (vdW) structure enable excellent mechanical and electrical performance for flexible electrodes and electronics and might be a candidate for MIR regulation. However, current techniques for preparing vdW graphene films require binder or solution assistance, resulting in chemical residues and performance degradation. Here, a new strategy for preparing large-area vdW graphene films by simple mechanical adhesion without any additives was proposed. By selecting the carriers and substrates with proper fracture energies, graphene nanosheets can be transferred from one polymer to another with a layer-by-layer structure. The obtained graphene films possess desired thickness and comparable electrical conductivity (92.8 $\pm$ 4.6 ohm sq^{-1}) with those by chemical vapor deposition. They are of high compactness even for ions to intercalate reversibly, which exhibit excellent electrochemical activity and electro-optical regulation capability, effectively suppressing 90% thermal radiation. This strategy can be extended to prepare high-performance vdW graphene films on various polymer substrates and used for sustainable and smart electro-optical applications.

KEYWORDS

dynamic emissivity, electrochemical device, graphene, thermal camouflage, van der Waals film

1 | INTRODUCTION

MIR-regulating materials, also called thermal regulating materials, are gaining growing attention due to the thermal management behavior in radiative cooling,[1] personal thermal management,[2–4] thermal camouflage,[5,6] communication,[7,8] and food packaging.[9] Such materials can manipulate the thermal radiation (P) either by emissivity

(ε) engineering or surface temperature (T) engineering according to Stefan Boltzmann Law ($P = \varepsilon\sigma T^4$).[10,11] Compared to surface temperature regulating materials such as phase change materials, emissivity engineering materials proposed an intrinsic solution to regulate thermal radiation, which would not influence the thermal sensation caused by improper temperature.[10] Current emissivity regulating materials mainly include vanadium dioxide,[12] $Ge_2Sb_2Te_5$,[13] perovskite oxides,[14] tungsten oxides,[15] polyaniline,[16] poly(3,4-ethylene dioxythiophene),[17] carbon nanotubes,[2,8] and graphene.[18,19]

Graphene is regarded as a breakthrough for thermal regulation among all materials due to its two-dimensional structure, broadband absorption, and adjustable Fermi level which can be tuned by ionic intercalation into the interlayers with an efficient electrochemical structure.[5,20,21] Due to the poor regulation or electromagnetic shielding effect caused by inappropriate thickness, graphene films for the largest thermal modulation are anticipated to possess a certain thickness (100–150 layers). Such films with controlled thickness are generally produced by CVD or reduction.[5,7,22] However, the thermal regulation performance of reduced graphene oxide films was unsatisfactory due to the graphene structure's high defect density. CVD-grown graphene films exhibit excellent emissivity regulation because of the fine structure; however, it is hard to realize scalable production and practical application due to the long synthesis duration, complex etching of metal substrates, transfer process, and surface fracture during use.[23] For graphene to be employed as a thermal regulator, it is crucial to identify graphene synthesis with the appropriate thickness, low defect density, and simple, scalable manufacturing.

van der Waals (vdW) films possess exceptional electrical and mechanical characteristics due to the large width-to-thickness ratio and the vast area of plane-to-plane vdW contact between neighboring sheets.[24–26] 2D materials such as graphene,[27,28] MXene,[29] MoS_2,[30] black phosphorus,[31] and BN[32] have been synthesized into vdW films utilizing the intermolecular forces by spin coating,[33,34] layer-by-layer assembly,[35,36] spray coating,[26,29] and inkjet printing.[37] The nanosheets assemble into continuous films with adjacent sheets interacting through vdW forces with merely interfacial trapping, resulting in excellent electrical conductivity.[24] Such performance makes vdW graphene film (vdWGRf) a good candidate for MIR regulating. However, prior techniques for vdW films' formulation rely on binders and solution assistance, limiting its production and causing solution waste. In addition, excess or residual impurities also bring performance degradation.

Here, we proposed a novel strategy to prepare Scalable Van Der Waals Graphene Films for Electro-Optical Regulation (vdWGRfs) without binder and solution assistance and applicate the vdWGRfs to thermal regulation. By selecting interfacial fracture energies with graphene nanosheets, vdWGRfs can be directly prepared on variable polymer substrates (e.g., polytetrafluoroethylene, PTFE; Polydimethylsiloxane, PDMS; Nafion®). Through a repeated dragging–adhesion–separation process, graphene nanosheets are able to stack in layers and form vdWGRfs. Such mechanical adhesion method is scalable, cost-effective (0.3 USD m^{-2}), room-temperature processable, binder-, and solvent-free. The electrical conductivity (sheet resistance to 92.8 ± 4.6 ohms sq^{-1}) and flexibility (bend radius to 0.5 mm) of the as prepared vdWGRfs are comparable to multilayer graphene films grown by CVD; however, they are more cost-effective and resistant to fracture. Later, a PTFE-based vdWGRf was directly assembled into an electrochemical device by injecting 1-ethyl-3-methylimidazolium bis(trifluoromethylsulfonyl)imide (EMIMTFSI) into the porous PTFE substrate. The electrochemical device demonstrated the excellent thermal regulation capability of suppressing 90% radiative heat transfer and reducing the emissivity from 0.6 to 0.1. The emissivity regulation arising from the ion intercalation into graphene interlayers was determined by in situ x ray diffraction (XRD). Due to the capacitor intrinsic of the thermal regulator, a corrected working voltage range of −0.5 to 4 V was provided, resulting in excellent stability with 90% modulation retention in 300 cycles. The facile and scalable production strategy for high-performance vdWGRf may facilitate the practical application of graphene as flexible electrodes and thermal regulators, such as personal thermal management, radiative cooling, and thermal camouflage.

2 | RESULTS AND DISCUSSION

2.1 | Mechanical adhesion to prepare vdWGRfs

Direct preparation of thin films on flexible plastic substrates facilitates sensing, storage, and communication functions for electrical devices.[38] Here, we proposed a scalable production strategy of vdWGRfs directly on polymer substrates without binder and solution assistance via a simple mechanical adhesion method. Graphene nanosheets adsorbed by a carrier polymer film could be transferred to a substrate polymer film by a dragging–adhesion–separation process (Figure 1A[i–iii]). By repeating the process, graphene nanosheets could be accumulated on the substrate, and a graphene film could finally be formed (Figure 1A[iv–vi]). The only existed three objects (graphene nanosheets, polymer carrier, polymer substrate) and simple external force make it necessary to believe that graphene film can be formed by a simple

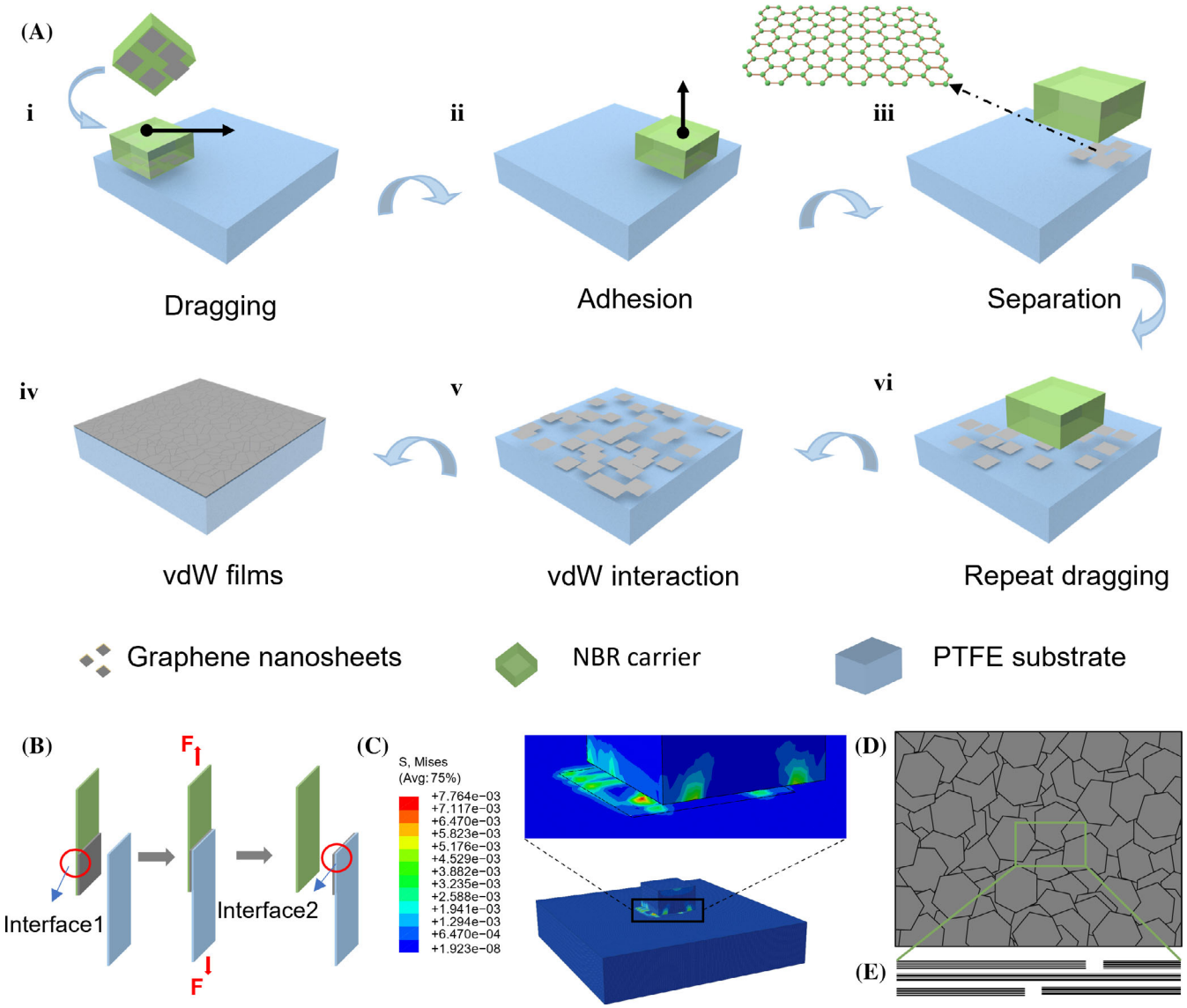

FIGURE 1 Mechanical adhesion method to prepare vdWGRfs. (A) Schematic of the mechanical adhesion method. (i) Graphene nanosheets were adhered onto a nitrile butadiene rubber (NBR) carrier and being dragged onto the PTFE substrate; (ii) Graphene nanosheets transferred from the NBR carrier to the PTFE substrate by dragging; (iii) The polymer carrier was removed, and the graphene nanosheets were separated with the polymer carrier; (iv) Repeated the dragging–adhesion–separation process; (v) Graphene nanosheets remained on the PTFE substrate by vdW force; (vi) vdWGRf formation. (B) Sketch of the graphene nanosheets transfer process. Interface1 and Interface2 demonstrate the interface of graphene nanosheets and polymer carrier, interface of graphene nanosheets and substrate film, respectively. F is the applied force. (C) Debonding simulation of the interface between the polymer carrier and graphene nanosheets: von Mises Stress state of the graphene nanosheets transfer process. Schematic of vdWGRf with stacking layer-by-layer structure: (D) Top view and (E) cross-section view.

mechanical adhesion, which is similar to the mechanical exfoliation of graphene nanosheets from graphite. To explore the mechanics, we conducted finite element analysis on the system stress during the dragging–adhesion–separation process based on traction-separation criteria (more information in Figure S1). It was found that the transfer can happen while the fracture energy of Interface1 (graphene nanosheets and polymer carrier) was lower than that of Interface2 (graphene nanosheets and polymer substrate) (Figure 1B). In addition, the surface energies of the graphene nanosheets and the polymer substrates should be similar, which is essential for the layer-by-layer structure. In an NBR carrier and PTFE substrate system, graphene nanosheets started to transfer when the strain energy release rate reached the interfacial fracture energy (Figure S2). The simulation result (Figure 1C) demonstrated that the Interface1 was detached, with graphene remaining on the PTFE

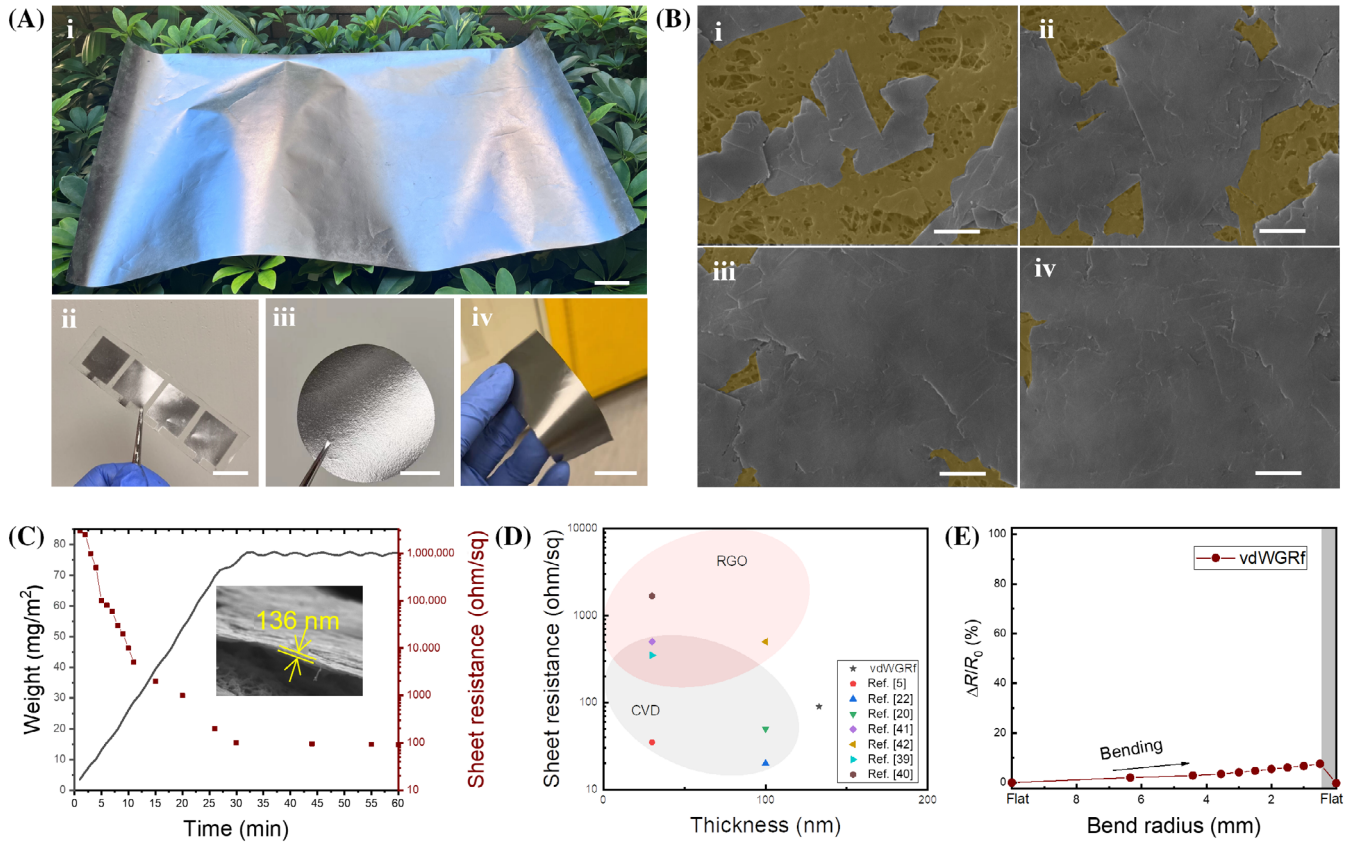

FIGURE 2 Morphology and electrical performance of vdWGRfs. (A) Photographs of vdWGRfs demonstrated on (i) large (40 cm * 80 cm), (ii) smooth (Nafion®), (iii) porous (PTFE), and (iv) elastic (PDMS) substrates, respectively. Scale bars, 5, 1, 1, and 1 cm, respectively. (B) Sequential scanning electron microscopy images of the vdWGRfs formation on a porous PTFE substrate. Scale bars, 2 μm. (C) Weight variation and sheet resistance of the PTFE-based vdWGRfs with preparation time increases. (D) Ashby plot comparing the sheet resistance of the vdWGRfs to previously reported graphene films by CVD and reduction method.[5,20,22,39–42] (E) Electrical resistance variation of the PTFE-based vdWGRf at a bend radius up to 0.5 mm.

substrate. The mechanical adhesion method is also applicable on other substrates, such as PDMS and Nafion®, where the fracture energies of Interface1 are lower than that of Interface2 (more information in Section 4). Using such method, vdWGRfs were prepared with stacking structure (Figure 1D,E).

2.2 | Performance of vdWGRfs

By selecting the carriers and substrates with proper fracture energies, vdWGRfs can be obtained on various substrates with arbitrary dimensions. We demonstrated flexible vdWGRfs with a dimension of 80 cm length and 40 cm width (Figure 2A[i]) and on smooth (Figure 2A[ii]), porous (Figure 2A[iii]), and stretchable substrates (Figure 2A[iv]), respectively. All vdWGRfs exhibited strong metallic luster, associated with the layer-by-layer stacking structure and high electrical properties. The structure of a PTFE-based vdWGRf was determined by sequential SEM images, finding that graphene nanosheets assembled onto the porous substrate layer by layer (Figure 2B[i–iii]), entirely and flatly adhered onto the PTFE substrate without any part upturned or detached, forming a vdWGRf (Figure 2B[iv]). Under MIR spectral testing, vdWGRfs exhibited no obvious absorption peaks and showed almost the same reflectance at different positions, proving all carbon structures and high uniformity (Figure S3). X-ray photoelectron spectroscopy (XPS) characterizations proved the high carbon content and fine graphene structure of graphene nanosheets (Figure S4), resulting in ultra-low defects of the vdWGRfs, where the values of I_D/I_G (0.20) that evaluate the graphite structure defect degree are nearly the same as the pristine graphene nanosheets ($I_D/I_G = 0.08$), approved by Raman spectra (Figure S5). Also, the impurity-free structure of vdWGRfs was determined by XRD (Figure S6). It is important to note that the thickness of the vdWGRf cannot grow indefinitely, which is limited by the shear force.[43] With the loading content of graphene nanosheets increasing to ~75 mg m^{-2}, the

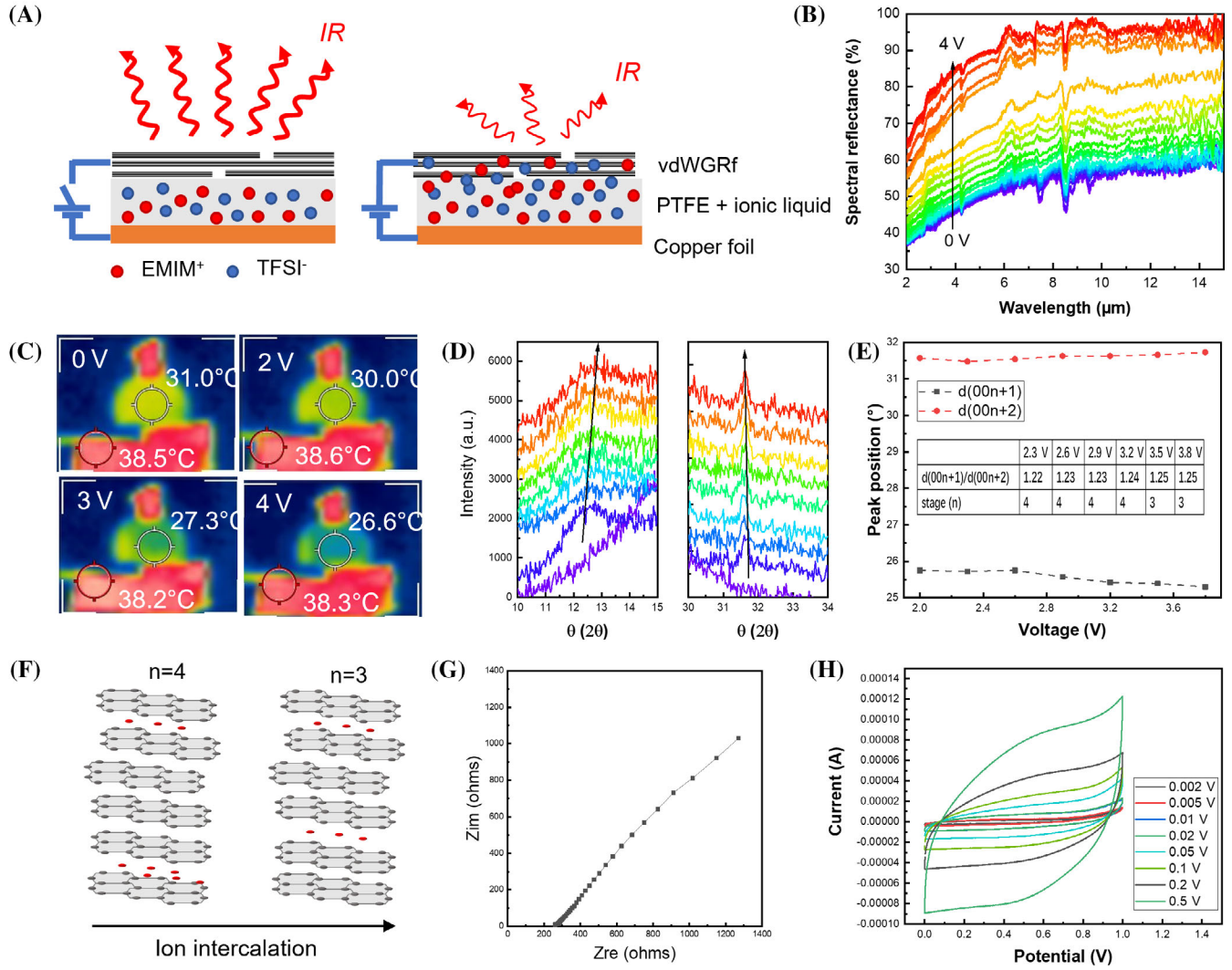

	2.3 V	2.6 V	2.9 V	3.2 V	3.5 V	3.8 V
d(00n+1)/d(00n+2)	1.22	1.23	1.23	1.24	1.25	1.25
stage (n)	4	4	4	4	3	3

FIGURE 3 Performance of a vdWGRf-based electrochemical device. (A) Schematic of the device structure with voltage off (left, high thermal radiation) and voltage on (right, low thermal radiation). PTFE-based vdWGRf is injected with EMIMTFSI ionic liquid and then adhered with a copper film. (B) Spectral reflectance in the wavelength of 2–15 μm as a function of 0–4 V applied voltage. (C) Thermal images of the vdWGRf-based electrochemical device on a 38°C hot plate under room temperature of 26°C. (D) In situ XRD spectra of the vdWGRf-based electrochemical device under 0–3.4 V. (E) XRD peak positions $(00n + 1)$, $(00n + 2)$ of the charged vdWGRf-based thermal regulator. Insert table shows the ratio of the two peak positions and the corresponding stage phase of vdWGRf. (F) Schematic of ions intercalation stages into graphene layers. (G) Nyquist plot of the vdWGRf-based solid electrochemical device. (H) CV curves of the vdWGRf-based solid electrochemical device at scan rates from 0.002 to 0.5 V.

thickness stopped growing (Figure 2C). The thickness of vdWGRfs was around 136 nm, determined by SEM (Figure 2C), which was exactly in line with the theoretical calculation and thickness to achieve the theoretical maximum emissivity regulation of graphene film with 100–150 layers.[22,44]

The ultra-low defect and impurity-free vdW structure endow the vdWGRfs with excellent mechanical and electrical properties. Here, the sheet resistance of vdWGRfs was 92.8 ± 4.6 ohm sq^{-1} at a maximum thickness (Figure 2C). The electrical conductivity of vdWGRfs was comparable with CVD-grown graphene films with 100–150 nm thickness of 20–100 ohm sq^{-1} [5,45] but much lower than that of reduced graphene oxide films of ~1000 ohm sq^{-1} [46] (Figure 2D). The high electrical conductivity arises from the ultralow carrier barrier of graphene nanosheets' highly compact vdW structure with the dangling-bond-free interface.[47] In addition, the vdWGRf showed excellent mechanical properties, with a maximum 7% electrical resistance change up to a 0.5 mm bend radius (Figure 2E). After bending for 5000 cycles at a 2.5 mm bend radius, there was no obvious change in

electrical resistance and morphology (Figure S7), indicating that the vdW structure maintained well.

2.3 | Performance of a vdWGRf-based electrochemical device

The PTFE-based vdWGRf was fabricated into an electrochemical device, where vdWGRf acted as the working electrode layer, porous PTFE film directly functioned as the separator, ionic liquid EMIMTFSI worked as the electrolyte, and a copper foil served as the counter electrode (Figure 3A). By applying appropriate voltage on the electrochemical device, the ions will intercalate into the graphene layers, resulting in a change in the Fermi energy and carrier density, which alters graphene's optical properties. The optical properties in MIR wavelength, associated with the thermal radiation, were measured quantitively to examine the dynamic spectrum of the vdWGRf. A failure voltage of 5 V was first determined, with MIR reflectance decreased significantly (Figure S8). The spectral reflectance of the vdWGRf-based electro-optical device was tested under an efficient working voltage of 0–4.4 V (Figure 3B), and the integrated emissivity with voltage variation under two atmospheric windows (3–5 μm and 8–13 μm) was determined (Figure S9). An ultra-low emissivity of 0.1 was detected at 4 V, which means the thermal radiation of the vdWGRf can be suppressed to a very low value. Thermal images were taken to visually observe the dynamic thermal radiation of vdWGRf, by a homemade apparatus composed of a hot plate and a thermal camera (Figure S10). The apparent temperature of the vdWGRf decreased by 5.4°C from 31 to 26.6°C in a normal indoor environment of 26°C (Figure 3C) and the electro-optical regulation sustained for about 44 min. A spectral test was studied to determine the working principle of the vdWGRf thermal regulator. In situ XRD of the vdWGRf thermal regulator was tested under an effective working voltage of 0–4 V with three characteristic peaks of PTFE observed at 18.22°, 22.74°, and 25.98°. The C002 peak of graphene was observed at 26.5°. (Figure S10) The C002 peak weakened after the applied voltage exceeded 2 V, and two new peaks (00n + 1) and (00n + 2) appeared as a signal of TFSI anions' intercalating into graphene layers (Figure S11 and Figure 3D), where n represented the intercalating layers followed by n layers of pristine graphene.[48] The ratio of these two peaks' position d(00n + 1)/d(00n + 2) was used to value the stage phase *n* (Figure 3E). When the voltage reached 2.3 V, a stage phase 4 graphene intercalation compound was observed, and a stage phase 3 reached at 3.5 V. Compared to a CVD-grown graphene-based thermal regulator, the vdWGRf-based thermal regulator demonstrated a lower intercalation stage, which contributes to the composited few-layer graphene nanosheets.[22] The results indicated that the ions intercalated into graphene layers under electrical voltage, resulting in the MIR property change (Figure 3F).

The vdW structure of graphene film may optimize its electroactive surface and endow vdWGRf energy and charge storage capacities. The electrochemical properties were evaluated to explore the nature of the vdWGRf thermal regulator, including electrochemical impedance spectroscopy (EIS), cyclic voltammetry (CV), galvanostatic charge/discharge (GCD), capacitance, and stability. EIS suggested that the impedance of the ion dispersion was low (Figure 3G). At all scan rates, the CV curves of the all-solid vdWGRf-based thermal modulator exhibited quasi-rectangle shapes and instantaneous current response to voltage reversal, demonstrating the electrochemical activity (Figure 3H). The specific capacitance of the device was calculated, with a maximum value of 16.95 F g^{-1} at the scan rate of 0.002 V s^{-1} (Figure S12). Compared to a CVD-grown multilayer graphene-based device with the same structure, the vdWGRf-based device exhibited a little larger capacitance due to the stacking vdW structure.[44] GCD curves measured under the current of 10–60 μA (Figure S12) with triangle shapes determined the formation of efficient electric double layers and further confirmed the capacitor nature of the vdWGRf-based emissivity modulator. The capacitor nature of the vdWGRf and the electrical current hysteresis effect suggested that a proper reverse voltage might be applied to the thermal regulator to release the accumulated ions. Besides, the lifetime test of the device with no significant decrease in both capacitance and voltage demonstrated stability in 100 cycles (Figure S13).

2.4 | Electro-optical regulation and large-area thermal camouflage

Working as a large-area thermal regulating material, the response time and the apparent temperature regulation of the vdWGRf-based thermal regulator were tested. With a pulse voltage changed at the 10th second from 0 to 4 V, it took around 7 s to steady the apparent temperature from 30.2 to 26.1°C, demonstrating a relatively fast response (Figure 4A). Due to the capacitor nature of the vdWGRf-based thermal regulator, a slightly negative voltage of 0.5 V was settled to release the accumulated cations on the vdWGRf. The stability of the regulator in 300 cycles was tested, finding that the thermal regulator maintained excellent emissivity regulating capability with 90% retention in 300 cycles (Figure 4B). The emissivity

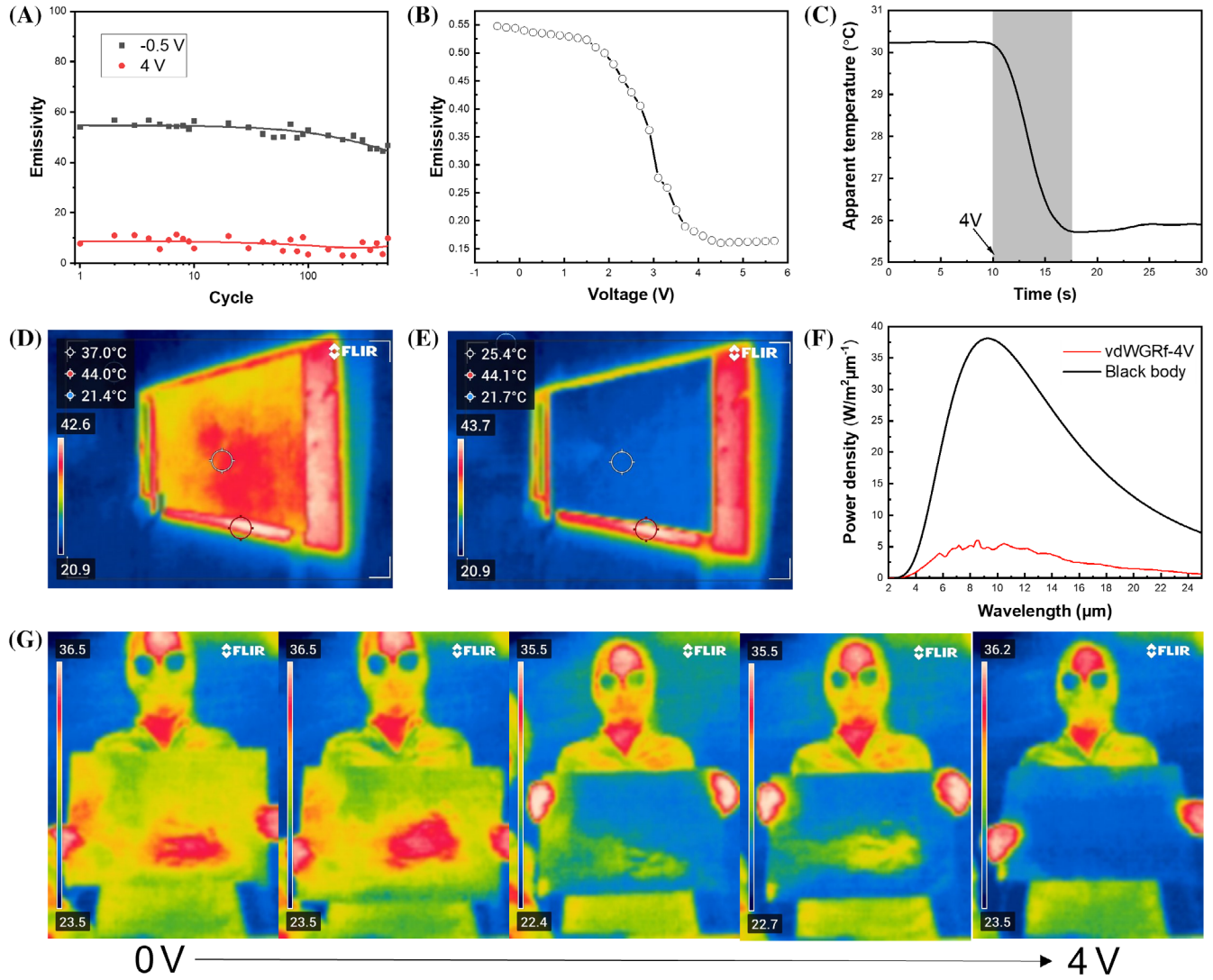

FIGURE 4 MIR regulating and thermal camouflage of large area vdWGRfs. (A) Apparent temperature change under a 0–4 V transition at the 10th second. (B) Emissivity regulation stability in 300 cycles with an applied voltage of −0.5 to 4 V. (C) The Integrated emissivity of the vdWGRf-based thermal regulator at the 300th cycle in 2–15 μm. Thermal images of the vdWGRf-based thermal regulator at (D) 0 V and (E) 4 V on a 45°C hotplate. (F) Blackbody radiation and radiation power emitted from the vdWGRf-based thermal regulator at 4 V. (G) Thermal camouflage demonstration of the vdWGRf under sequential 0–4 V on a human body. Dimension: 30 cm width and 40 cm length.

regulation at the 300th cycle was tested under −0.5 to 4 V, maintaining 0.4 emissivity regulation (Figure 4C). A large area electrically responsive thermal camouflage system with vdWGRf on a 45°C hot plate was demonstrated, which could conceal perfectly under the thermal camera because of the lower emissivity at 4 V than the background (Figure 4D,E). It is because the regulated emissivity of vdWGRf (value of 0.15) is lower than that of the background, and the thermal radiation emitted from the vdWGRf at 4 V was only 10% of the black body thermal radiation (Figure 4F). In addition, a camouflage demonstration on the human body at room temperature (∼25°C) was shown (Figure 4G). The vdWGRf-based thermal regulator can obviously change the apparent temperature of the human body from warm to cold, which is almost consistent with the background temperature and can be used to resist the detection of a thermal detector.

3 | CONCLUSION

To conclude, we proposed a new mechanical adhesion strategy of van der Waals graphene thin films and applied it to electro-optical regulation. By repeating the adhesion–dragging–separation process, vdWGRfs can be synthesized on various substrates such as PTFE, PDMS,

and Nafion®. The vdWGRfs are flexible and highly electrically conductive with a sheet resistance of 92.8 ± 4.6 ohm sq^{-1}, and the preparation is low-cost, binder- and solution-free, large-area, room-temperature processable. Further, the vdWGRf was assembled into an electrochemical thermal regulator, with vdWGRf as the thermal regulating layer, PTFE as the separator, EMIMTFSI as the electrolyte, and copper foil as the counter electrode. The emissivity of the regulator was suppressed from 0.6 to 0.1 in an efficient working voltage of 0–4 V. The vdWGRf-based thermal modulator can nearly decrease the apparent temperature to that of the surrounding, acting as a perfect thermal camouflage surface. In addition, it can reduce 90% of radiative heat transfer, which can be used for thermal management. To avoid the ions' retention under the charging and discharging process, the working voltage of the thermal regulator was adjusted from −0.5 to 4 V, resulting in excellent stability with 90% modulation retention in 300 cycles. The facile and scalable production strategy for high-performance vdWGRf may facilitate the practical application of graphene as flexible electrodes and thermal regulators, such as personal thermal management, radiative cooling, and thermal camouflage.

4 | EXPERIMENTAL SECTION

4.1 | Materials

Graphene nanosheets with 5–8 layers, 95% carbon content, and 3–10 μm lateral diameter were purchased from China Graphene Institute. Ionic liquid, EMIMTFSI, was purchased from Tokyo Chemical Industry Co., Ltd. PTFE porous film with 20 μm thickness, 45% porosity, and pores with 100 nm diameter purchased from Asahi Kasei Co. was used as the polymer substrate and to contain ionic liquid. PDMS film 30 μm thickness was purchased from Hangzhou Westru Technology Co. Ltd. A commercial Nafion® film composited of sulfonated tetrafluoroethylene-based fluoropolymer-copolymer from DuPont was also used as the polymer substrate.

4.2 | Preparation of vdWGRfs

Firstly, graphene nanosheets adhered to a polymer carrier film by adhesion. In this research, NBR is utilized as the polymer carrier film. After dragging the polymer carrier with a horizontal force, the graphene nanosheets were transferred from the polymer carrier film and adhered to the PTFE substrate. Then, the polymer carrier film was separated with the PTFE substrate, and the dragging–adhesion–separation process was repeated. By repeating the process, graphene nanosheets adhered to the PTFE substrate and onto the graphene nanosheet-formed graphene film by vdW interaction. Finally, the vdWGRf is obtained. PDMS and Nafion® were also used as polymer substrates.

4.3 | Fabrication of vdWGRf-based electrochemical device

The vdWGRf-based thermal regulator comprised a PTFE-vdWGRf working electrode (3 cm*3 cm), 20 μL [EMIM]TFSI ionic liquid electrolyte, and a 3 cm*3 cm copper conductive tape counter electrode layer. The vdWGRf side was connected to a positive voltage, and the copper conductive tape was connected to a negative voltage.

4.4 | Characterizations

SEM images were taken by Tescan VEGA. Sheet resistance was tested using a KDY-1 four-probe square resistance tester with probes attached to the vdWGRfs at 10 random positions. Raman was performed under a 532 nm laser with Renishaw Micro-Raman Spectroscopy System. XPS spectra were obtained using ThermoFisher ESCALAB 250Xi. In situ XRD was performed with Rigaku SmartLab 9 kW. The Electrochemical test, including CV, EIS, and GCD, was performed by Versa STAT3 electrochemical workstation. The specific capacitance (C_s) for the graphene-based soft actuator was calculated according to the following equation:

$$C_s = \int \frac{1}{m} dV / \nu \Delta V$$

where, m is the total mass of the active material (g, graphene), ΔV is the potential window (V), ν is the scan rate (mV s^{-1}).

4.5 | Bending test

PTFE-based vdWGRfs with 1 cm width and 3 cm length were used for the bending test. A homemade bending machine and a Keithley 2400 source meter were used to test the electrical resistance of a 1 cm length.

4.6 | Electro-optical test and thermal images

MIR reflection was performed under an FTIR (Spectrum 100, PerkinElmer) with an integrating sphere. The

thermal images of vdWGRfs were taken by a FLIR C3-X thermal camera with an emissivity setting of 0.95 and a testing distance of 50 cm.

4.7 | Finite element analysis

The formation of vdWGRf was simulated by Finite Element Analysis. The simulation of the debonding of the interface between the polymer carrier and graphene nanosheets and the mechanical response was implemented in the commercial software ABAQUS 2017. Compared with the PTFE and the polymer carrier domain, the thickness of the interface between the graphene nanosheets and the polymer carrier was small enough and could be ignored. The fracture process area of the interfacial crack was defined using the zero-thickness cohesive element. The stiffness of the cohesive was specified as 1000 to ensure the rigid connection of materials on both sides of the interface. The damage initiation was captured by using the Maxs damage criterion, and the damage evolution was defined by using the energy criterion. The FEM is meshed using the Eight-node brick element with reduced integration (C3D8R) elements with fine size. The elastic modulus E and Poisson's ratio υ were $E_{PTFE} = 0.28$ GPa, $\upsilon_{PTFE} = 0.4$ for PTFE, $E_{NBR} = 4 \times 10^{-4}$ GPa, $\upsilon_{NBR} = 0.45$ for NBR, $E_{graphene} = 1000$ GPa, $\upsilon_{graphene} = 0.3$ for graphene nanosheet, $E_{PDMS} = 6 \times 10^{-3}$ GPa, $\upsilon_{PDMS} = 0.42$ for PDMS, $E_{Nafion} = 0.246$ GPa, $\upsilon_{Nafion} = 0.3$ for Nafion, respectively. The fracture energy of interfacial zones $G_{C1} = 100$–$300\ \mathrm{mJ\ m^{-2}}$ for the interface between PTFE and graphene nanosheet, $G_{C2} = 25$–$30\ \mathrm{mJ\ m^{-2}}$ for the interface between NBR and graphene nanosheet, 50–$60\ \mathrm{mJ\ m^{-2}}$ for the interface between PDMS and graphene nanosheet, respectively. The boundary condition of the dragging was to constrain the freedom of the bottom surface nodes of the PTFE substrate and impose a displacement vector in the XY plane.

4.8 | Calculation of the integrated emissivity and thermal radiation

Due to the opaque nature of the device, the integrated emissivity (ε) of the device was calculated by weighting $(1-R(\lambda))$ by the formula:

$$\varepsilon = \frac{\int_{\lambda_{\min}}^{\lambda_{\max}} (1-R(\lambda))B(\lambda)d\lambda}{\int_{\lambda_{\min}}^{\lambda_{\max}} B(\lambda)d(\lambda)}$$

where, λ is the wavelength, $B(\lambda)$ is the blackbody radiation for a particular wavelength and over the entire measured wavelength range according to the formula:

$$B(\lambda) = \frac{C_1\lambda^{-5}}{\exp[C_2/\lambda T]-1}$$

where, C_1 is the first radiation constant ($3.7418 \times 108\ \mathrm{W\ \mu m^4\ m^{-2}}$), C_2 is the second radiation constant ($1.4388 \times 10^4\ \mu\mathrm{m\ K}$), and T is the temperature.

ACKNOWLEDGMENTS

The authors would like to thank the Shenzhen-Hong Kong-Macao Science and Technology Plan Project (SGDX2020110309520101), Research Grants Council of Hong Kong (15302121), National Natural Science Foundation of China (21975214), National Key R&D Program of China (2018YFC2000900), Seed Fund of Research Institute of Intelligent Wearable Systems (CD45), Start-up Fund of The Hong Kong Polytechnic University (BE1H), Departmental General Research Fund of The Hong Kong Polytechnic University (UAME).

CONFLICT OF INTEREST STATEMENT

The authors declare no conflict of interest.

ORCID

Xujiang Chao https://orcid.org/0000-0002-0841-1790
Wei Chen https://orcid.org/0000-0001-9527-110X

REFERENCES

1. Yin X, Yang R, Tan G, Fan S. Terrestrial radiative cooling: using the cold universe as a renewable and sustainable energy source. *Science*. 2020;370(6518):786-791.
2. Zhang XA, Yu S, Xu B, et al. Dynamic gating of infrared radiation in a textile. *Science*. 2019;363(6427):619-623.
3. Hu R, Liu Y, Shin S, et al. Emerging materials and strategies for personal thermal management. *Adv Energy Mater*. 2020;10(17):1903921.
4. Peng Y, Cui Y. Advanced textiles for personal thermal management and energy. *Joule*. 2020;4(4):724-742.
5. Salihoglu O, Uzlu HB, Yakar O, et al. Graphene-based adaptive thermal camouflage. *Nano Lett*. 2018;18(7):4541-4548.
6. Li M, Liu D, Cheng H, Peng L, Zu M. Manipulating metals for adaptive thermal camouflage. *Sci Adv*. 2020;6(22):3494.
7. Ergoktas MS, Bakan G, Steiner P, et al. Graphene-enabled adaptive infrared textiles. *Nano Lett*. 2020;20(7):5346-5352.
8. Sun Y, Chang H, Hu J, et al. Large-scale multifunctional carbon nanotube thin film as effective mid-infrared radiation modulator with long-term stability. *Adv Opt Mater*. 2020;9(3):2001216.
9. Badshah MA, Leung EM, Liu P, Strzelecka AA, Gorodetsky AA. Scalable manufacturing of sustainable packaging materials with tunable thermoregulability. *Nat Sustain*. 2022;5(5):434-443.

10. Li Z, Chen W. Progress in dynamic emissivity regulation: control methods, material systems, and applications. *Mater Chem Front*. 2021;5(17):6315-6332.
11. Zhai H, Fan D, Li Q. Dynamic radiation regulations for thermal comfort. *Nano Energy*. 2022;100:107435.
12. Xiao L, Ma H, Liu J, et al. Fast adaptive thermal camouflage based on flexible VO_2/graphene/CNT thin films. *Nano Lett*. 2015;15(12):8365-8370.
13. Du KK, Li Q, Lyu YB, et al. Control over emissivity of zero-static-power thermal emitters based on phase-changing material GST. *Light Sci Appl*. 2017;6(1):e16194.
14. Park Y-S, Guo S, Makarov NS, Klimov VI. Room temperature single-photon emission from individual perovskite quantum dots. *ACS Nano*. 2015;9(10):10386-10393.
15. Lee SJ, Choi DS, Kang SH, et al. VO_2/WO_3-based hybrid smart windows with thermochromic and electrochromic properties. *ACS Sustain Chem Eng*. 2019;7(7):7111-7117.
16. Xu G, Zhang L, Wang B, et al. A visible-to-infrared broadband flexible electrochromic device based polyaniline for simultaneously variable optical and thermal management. *Solar Energy Mater Sol Cells*. 2020;208:110356.
17. Brooke R, Mitraka E, Sardar S, et al. Infrared electrochromic conducting polymer devices. *J Mater Chem C*. 2017;5(23):5824-5830.
18. Li W, Chen B, Meng C, et al. Ultrafast all-optical graphene modulator. *Nano Lett*. 2014;14(2):955-959.
19. Phan L, Walkup WG, Ordinario DD, et al. Reconfigurable infrared camouflage coatings from a cephalopod protein. *Adv Mater*. 2013;25(39):5621-5625.
20. Ergoktas MS, Bakan G, Kovalska E, et al. Multispectral graphene-based electro-optical surfaces with reversible tunability from visible to microwave wavelengths. *Nat Photonics*. 2021;15(7):493-498.
21. Huang H, Li J, Ke H, et al. Impact of ionic liquids on effectiveness of tuning the emissivity of multilayer graphene. *ACS Appl Mater Interfaces*. 2021;13(22):26256-26263.
22. Sun Y, Wang Y, Zhang C, et al. Flexible mid-infrared radiation modulator with multilayer graphene thin film by ionic liquid gating. *ACS Appl Mater Interfaces*. 2019;11(14):13538-13544.
23. Cui T, Yip K, Hassan A, et al. Graphene fatigue through van der Waals interactions. *Sci Adv*. 2020;6(42):eabb1335.
24. Lin Z, Huang Y, Duan X. Van der Waals thin-film electronics. *Nat Electron*. 2019;2(9):378-388.
25. Wang P, Jia C, Huang Y, Duan X. Van der Waals heterostructures by design: from 1D and 2D to 3D. *Matter*. 2021;4(2):552-581.
26. Zhong J, Sun W, Wei Q, Qian X, Cheng HM, Ren W. Efficient and scalable synthesis of highly aligned and compact two-dimensional nanosheet films with record performances. *Nat Commun*. 2018;9(1):3484.
27. Liu F, Navaraj WT, Yogeswaran N, Gregory DH, Dahiya R. Van der Waals contact engineering of graphene field-effect transistors for large-area flexible electronics. *ACS Nano*. 2019;13(3):3257-3268.
28. Zhang Z, Lin P, Liao Q, Kang Z, Si H, Zhang Y. Graphene-based mixed-dimensional van der Waals heterostructures for advanced optoelectronics. *Adv Mater*. 2019;31(37):e1806411.
29. Hantanasirisakul K, Zhao M-Q, Urbankowski P, et al. Fabrication of $Ti_3C_2T_x$ MXene transparent thin films with tunable optoelectronic properties. *Adv Electron Mater*. 2016;2(6):1600050.
30. Yan Z, Xu D, Lin Z, et al. Highly stretchable van der Waals thin films for adaptable and breathable electronic membranes. *Science*. 2022;375(6583):852-859.
31. Zong X, Hu H, Ouyang G, et al. Black phosphorus-based van der Waals heterostructures for mid-infrared light-emission applications. *Light Sci Appl*. 2020;9(1):1-8.
32. Zhu J, Kang J, Kang J, et al. Solution-processed dielectrics based on thickness-sorted two-dimensional hexagonal boron nitride nanosheets. *Nano Lett*. 2015;15(10):7029-7036.
33. Lin Z, Liu Y, Halim U, et al. Solution-processable 2D semiconductors for high-performance large-area electronics. *Nature*. 2018;562(7726):254-258.
34. Lin Z, Chen Y, Yin A, et al. Solution processable colloidal nanoplates as building blocks for high-performance electronic thin films on flexible substrates. *Nano Lett*. 2014;14(11):6547-6553.
35. Richardson JJ, Bjornmalm M, Caruso F. Multilayer assembly. Technology-driven layer-by-layer assembly of nanofilms. *Science*. 2015;348(6233):aaa2491.
36. Hong JY, Shin KY, Kwon OS, Kang H, Jang J. A strategy for fabricating single layer graphene sheets based on a layer-by-layer self-assembly. *Chem Commun*. 2011;47(25):7182-7184.
37. Carey T, Cacovich S, Divitini G, et al. Fully inkjet-printed two-dimensional material field-effect heterojunctions for wearable and textile electronics. *Nat Commun*. 2017;8(1):1202.
38. MacDonald WA. Latest advances in substrates for flexible electronics. *J Soc Inf Disp*. 2007;15(12):1075-1083.
39. Feng H, Cheng R, Zhao X, Duan X, Li J. A low-temperature method to produce highly reduced graphene oxide. *Nat Commun*. 2013;4(1):1539.
40. Wang J, Liang M, Fang Y, Qiu T, Zhang J, Zhi L. Rod-coating: towards large-area fabrication of uniform reduced graphene oxide films for flexible touch screens. *Adv Mater*. 2012;24(21):2874-2878.
41. Katagiri M, Miyazaki H, Yamazaki Y, et al. Electrical properties of multilayer graphene interconnects prepared by chemical vapor deposition; 2013. p. 1-3.
42. Liu J, Lin Z, Liu T, et al. Multilayer stacked low-temperature-reduced graphene oxide films: preparation, characterization, and application in polymer memory devices. *Small*. 2010;6(14):1536-1542.
43. Castilho CJ, Li D, Xie Y, Gao H, Hurt RH. Shear failure in supported two-dimensional nanosheet van der Waals thin films. *Carbon*. 2021;173:410-418.
44. Li Z, Balilonda A, Yang S, Tao X, Chen W. Graphene-based soft actuator with dynamic spectrum modulation for a smart thermal surface. *ACS Appl Nano Mater*. 2022;5(6):8298-8305.
45. Zhao L, Zhang R, Deng C, Peng Y, Jiang T. Tunable infrared emissivity in multilayer graphene by ionic liquid intercalation. *Nanomaterials*. 2019;9(8):1096.
46. Pei S, Zhao J, Du J, Ren W, Cheng H-M. Direct reduction of graphene oxide films into highly conductive and flexible graphene films by hydrohalic acids. *Carbon*. 2010;48(15):4466-4474.
47. Geim AK, Grigorieva IV. Van der Waals heterostructures. *Nature*. 2013;499(7459):419-425.

48. Schmuelling G, Placke T, Kloepsch R, et al. X-ray diffraction studies of the electrochemical intercalation of bis(trifluoromethanesulfonyl)imide anions into graphite for dual-ion cells. *J Power Sources*. 2013;239:563-571.

SUPPORTING INFORMATION

Additional supporting information can be found online in the Supporting Information section at the end of this article.

How to cite this article: Li Z, Chao X, Balilonda A, Chen W. Scalable van der Waals graphene films for electro-optical regulation and thermal camouflage. *InfoMat*. 2023;e12418. doi:10.1002/inf2.12418